american physiological society

JNP JOURNAL OF NEUROPHYSIOLOGY

J Neurophysiol 126: 653–667, 2021.
First published July 7, 2021; doi:10.1152/jn.00674.2020

RESEARCH ARTICLE

Computational Neuroscience

A model of metabolic supply-demand mismatch leading to secondary brain injury

Jiang-Ling Song,[1,2] Jennifer A. Kim,[3] Aaron F. Struck,[4,5] Rui Zhang,[1] and M. Brandon Westover[2]

[1]*The Medical Big Data Research Center, Northwest University, Xi'an, China;* [2]*Department of Neurology, Massachusetts General Hospital, Harvard Medical School, Boston, Massachusetts;* [3]*Department of Neurology, Yale New Haven Hospital, New Haven, Connecticut;* [4]*Departments of Neurology, University of Wisconsin–Madison, Madison, Wisconsin; and* [5]*William S Middleton Veterans Administration Hospital, Madison, Wisconsin*

Abstract

Secondary brain injury (SBI) is defined as new or worsening injury to the brain after an initial neurologic insult, such as hemorrhage, trauma, ischemic stroke, or infection. It is a common and potentially preventable complication following many types of primary brain injury (PBI). However, mechanistic details about how PBI leads to additional brain injury and evolves into SBI are poorly characterized. In this work, we propose a mechanistic model for the metabolic supply demand mismatch hypothesis (MSDMH) of SBI. Our model, based on the Hodgkin–Huxley model, supplemented with additional dynamics for extracellular potassium, oxygen concentration, and excitotoxity, provides a high-level unified explanation for why patients with acute brain injury frequently develop SBI. We investigate how decreased oxygen, increased extracellular potassium, excitotoxicity, and seizures can induce SBI and suggest three underlying paths for how events following PBI may lead to SBI. The proposed model also helps explain several important empirical observations, including the common association of acute brain injury with seizures, the association of seizures with tissue hypoxia and so on. In contrast to current practices which assume that ischemia plays the predominant role in SBI, our model suggests that metabolic crisis involved in SBI can also be nonischemic. Our findings offer a more comprehensive understanding of the complex interrelationship among potassium, oxygen, excitotoxicity, seizures, and SBI.

NEW & NOTEWORTHY We present a novel mechanistic model for the metabolic supply demand mismatch hypothesis (MSDMH), which attempts to explain why patients with acute brain injury frequently develop seizure activity and secondary brain injury (SBI). Specifically, we investigate how decreased oxygen, increased extracellular potassium, excitotoxicity, seizures, all common sequalae of primary brain injury (PBI), can induce SBI and suggest three underlying paths for how events following PBI may lead to SBI.

excitotoxicity; metabolic supply-demand mismatch hypothesis; neural computational model; secondary brain injury; seizures

INTRODUCTION

Secondary brain injury (SBI) is a common and potentially preventable complication following many types of primary brain injury (PBI), including ischemic stroke, traumatic brain injury (TBI), and subarachnoidal hemorrhage (SAH), etc. SBI occurs when, following an initial injury, additional neuronal damage develops and leads to a worsening of neurological symptoms and deficits, often followed by worsening of the long-term degree of neurologic disability (1).

In many cases, SBI involves a prolonged state of "metabolic crisis," in which signs of neuronal injury are accompanied by signs of increased metabolism (2–4). Metabolic crisis was originally assumed to be primarily caused by large-artery ischemia; however, recent work suggests that other factors play important roles. These include both factors that increase metabolic demand (e.g., seizures, periodic discharges, and cortical spreading depolarizations, Refs. 2 and 3) and factors that decrease metabolic supply (e.g., inflammation, microvascular spasm, microthrombosis, and impairment of local autoregulation). The "metabolic supply-demand mismatch hypothesis" (MSDMH) has been proposed as a conceptual framework to explain these findings (5). According to the MSDMH, when tissue injured by PBI (reduced supply) is recruited into

Correspondence: R. Zhang (rzhang@nwu.edu.cn); M. B. Westover (MWESTOVER@mgh.harvard.edu).
Submitted 2 December 2020 / Revised 29 June 2021 / Accepted 30 June 2021

metabolically demanding activity (increased demand), this compromises brain function, leading to tissue injury and neurologic deficits, which may be either reversible or irreversible depending on the severity and duration of the supply-demand mismatch. However, mechanistic details of how PBI leads to additional brain injury and evolves into SBI are poorly characterized.

A neural computational model is a kind of mathematical model based on biophysics, which is a tool for testing dynamic scenarios to gain mechanistic insight into the dynamics of brain activities. It can be categorized into two main families, macroscopic models and microscopic models, according to the level of biological organization they aim to represent. The former one focuses on describing the mean activities (such as mean firing rates, mean postsynaptic potentials) of neuronal populations (6–9). In contrast, the latter one focuses on quantifying the dynamical behavior of single neurons, which are considered to be the primary computational units of brain function (10–15). Compared with macroscopic models, the microscopic models are able to capture brain dynamics in a more realistically and biologically explanative way. The microscopic approach can be traced back to the 1950s with the seminal works of Hodgkin and Huxley, who described the model (i.e., HH model) to explain how nerve action potentials in the squid giant axon are initiated and propagated (16). This approach has then been progressively used to simulate various electrophysiological activities (e.g., event-related potential, α rhythm) and shed light on the mechanisms underlying both neurophysiological (e.g., attention, learning, speech perception) and pathological phenomena (e.g., epileptic seizures, sleep disorders).

Recent work on oxygen metabolism during and following epilepsy has shown that a modification of the HH model could simulate the seizure pattern (17). Seizures are a common phenomenon in SBI. Building on this work, this paper proposes a mechanistic model for the MSDMH of SBI. Our model, based on the Hodgkin–Huxley model, supplemented with additional dynamics of three known mechanisms in SBI, shows mechanistic details of how PBI leads to neuropathological alterations and evolves into SBI. Mechanisms applied here are believed to be central to brain dysfunction in SBI: *1*) decreased oxygen; *2*) increased extracellular potassium; and *3*) increased excitotoxicity. Based on the proposed model, we show how changes in extracellular potassium, oxygen concentration, and excitotoxicity might play important roles in the evolution from PBI to SBI and suggest three underlying pathways for how events following PBI may lead to SBI. The corresponding conceptual model is illustrated in Fig. 1. We also use the proposed model to explain several important observations in the literature, including: *1*) brain injury frequently leads to seizures and periodic discharges (PDs); *2*) seizures and PDs are associated with tissue hypoxia; and *3*) more severe brain injury is associated with more severe seizures and PDs (i.e., more frequent seizures, or higher frequency PDs).

MATERIALS AND METHODS

In this section, we provide background to motivate the proposed model and then give a mathematical description of our proposed SBI model (SBIM).

Background and Motivation

Increased extracellular potassium levels.

Increases in extracellular potassium ($[K^+]_o$) have been described after many types of PBI. Several prior studies indicate that a massive increase in $[K^+]_o$ occurs in response to experimental traumatic brain or spinal cord injury (18). In addition, in the early phase of ischemia, accumulation of extracellular K^+ also occurs, which is related to decreased blood flow and impairment of ionic pumps (19). It has also been shown in rats with SAH that the hemolysis products hemoglobin and extracellular K^+ accumulate as well in the subarachnoid space (20). An increase in $[K^+]_o$ has also been reported following concussive brain injury, which can be explained in terms of K^+ flux through voltage-gated K^+ channels associated with neuronal discharges, and several lines of evidence suggest that intense neuronal discharges occur immediately following concussive brain injury (21).

Decreased oxygen levels.

Several prior studies show that decreasing oxygen levels often accompany PBI and are likely involved in SBI. It has been shown both in experimental models and in human brain injury that cerebral metabolic rate of oxygen ($CMRO_2$) is reduced by at least 50% after TBI in the acute period (2, 22), which is thought to arise from a predominantly calcium-mediated impairment of mitochondrial respiratory function as well as early cell death. One study of SBI occurring in a patient with SAH demonstrated that cerebral blood flow (CBF) and $CMRO_2$ depression were evident in both hemispheres, although large vessel vasospasm was present in only one of the hemispheres (23). The decreased oxygen saturation in asymmetrically prominent cortical veins (APCV), correlating with an increase of deoxygenated hemoglobin, has also been seen in ischemic stroke (24).

Excitotoxicity.

Excitotoxicity induced by the presence of excessive excitatory amino acids (EAA) or neurotransmitters and receptor activation accompanies acute brain injury. Several lines of evidence indicate that activation of muscarinic cholinergic and/or NMDA glutamate receptors may significantly contribute to TBI pathophysiology (25), likely due to excessive release of neurotransmitters caused by TBI-induced membrane depolarization. Katayama et al. (26) reported a 90% increase in glutamate within 2 min after moderate TBI. A much larger magnitude of EAA release was reported by Faden et al. (27). In their study, moderate fluid-percussion TBI associated with contusions produced 282% and 273% increases in glutamate and aspartate, respectively, whereas severe injury produced increases of 940% and 1,849%. In ischemic stroke, excitotoxicity is considered to be a central mechanism as well. The reduction of blood flow supply to the brain during ischemic stroke results in membrane depolarization and activation of voltage-gated calcium channels, which lead to excessive release of EAA—particularly glutamate—to the extracellular compartment (28, 29).

Seizures and seizure-like brain activity.

Seizures are a major concern in the acute period following PBI. For example, up to 25% of patients with TBI (30), and

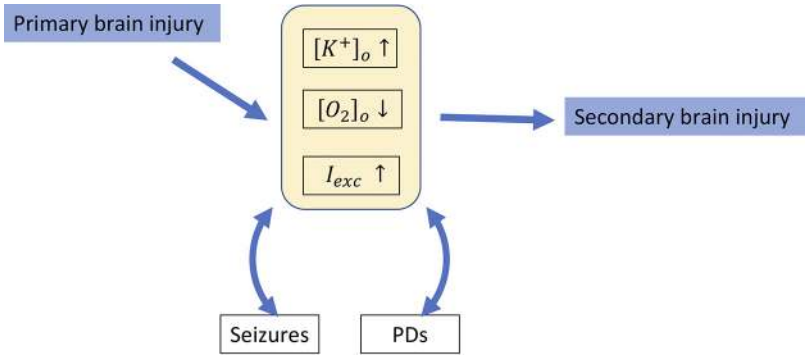

Figure 1. Conceptual model for how O_2 levels, extracellular K^+ levels, and excitotoxicity affect seizures and periodic discharges (PDs) to induce SBI. I_{exc}, excitatory synaptic current; $[K^+]_o$, extracellular potassium concentration; $[O_2]_o$, extracellular oxygen concentration; SBI, secondary brain injury.

12% of patients with subarachnoid hemorrhage (SAH), have acute electrographic seizures when monitored with electroencephalography (EEG) (31). Seizures are associated not only with heightened morbidity and mortality in early stages following TBI, but are also a leading risk factor for death several years following TBI (32). PDs are EEG patterns related to seizures commonly seen in patients with PBI (33). They are associated with an increased risk of seizures (34) and exhibit seizure-like properties including reversible focal neurophysiological dysfunction (35), as well as increased glucose metabolism and metabolic stress similar to seizures (5, 30).

The Hodgkin–Huxley Model

The Hodgkin–Huxley model (HH model) was proposed by Alan Lloyd Hodgkin and Andrew Fielding Huxley in 1952, which aims to explain the ionic mechanisms underlying the initiation and propagation of action potentials in the squid giant axon. We note that the full HH model is a set of partial differential equations, which include partial derivatives with respect to time and spatial position of the neuron (16). In this work, we consider only temporal dynamics and do not model spatio-temporal dynamics. Therefore, we use the "space-clamped" HH model, whose equations are formulated by

$$\frac{dV}{dt} = \frac{1}{C}(I_e - I_{Na} - I_K - I_{Cl}), \tag{1}$$

$$I_{Na} = G_{Na} m^3 h(V - E_{Na}) + G_{NaL}(V - E_{Na}), \tag{2}$$

$$I_K = G_K n^4 h(V - E_K) + G_{KL}(V - E_K), \tag{3}$$

$$I_{Cl} = G_{ClL}(V - E_{Cl}), \tag{4}$$

where V is the membrane potential; I_{Na} and I_K represent the sodium current and potassium current, whose values are the sum of the leak current and the current passing through certain channels respectively; I_{Cl} is the chloride leak current; I_e is the external applied current; G_{Na} and G_K represent the maximal conductance of sodium and potassium channels; G_{NaL}, G_{KL}, and G_{ClL} are the leak conductance of Na^+, K^+, and Cl^-, respectively; m, n, h denote the "gating" variables modeling the probability that a channel is open at a given moment in time. The combined action of m and h controls the Na^+ channels, whereas the action of n controls the K^+ channels. They can be described by

$$\frac{dm}{dt} = \alpha_m(1-m) - \beta_m m, \frac{dn}{dt} = \alpha_n(1-n) - \beta_n n, \frac{dh}{dt} = \alpha_h(1-h) - \beta_h h.$$

Here, α_i and β_i ($i = m, n, h$) represent the opening and closing rates of the ion channels, which depend on the membrane potential V shown as follows: $\alpha_m = \frac{0.32(54+V)}{1-\exp\left(-\frac{V+54}{4}\right)}$, $\alpha_n = \frac{0.032(52+V)}{1-\exp\left(-\frac{V+52}{5}\right)}$, $\alpha_h = 0.128\exp\left(-\frac{50+V}{18}\right)$, $\beta_m = \frac{0.28(27+V)}{\exp\left(\frac{V+27}{5}\right)-1}$, $\beta_n = 0.5\exp\left(-\frac{57+V}{40}\right)$, $\beta_h = \frac{4}{1+\exp\left(-\frac{V+27}{5}\right)}$.

Parameters E_{Na}, E_K, and E_{Cl} are reversal potentials of Na^+, K^+, and Cl^-, respectively, which are calculated according to Nernst equations in Ref. 36:

$$E_K = 26.64\ln\left(\frac{[K^+]_o}{[K^+]_i}\right), \tag{5}$$

$$E_{Na} = 26.64\ln\left(\frac{[Na^+]_o}{[Na^+]_i}\right), \tag{6}$$

$$E_{Cl} = 26.64\ln\left(\frac{[Cl^-]_i}{[Cl^-]_o}\right), \tag{7}$$

here, $[A]_i$ and $[A]_o$ represent the intracellular and extracellular concentration of ion A ($A \in \{Na^+, K^+, Cl^-\}$).

The Secondary Brain Injury Model

To better understand the effect of extracellular K^+ level, extracellular O_2 level, and excitotoxicity on SBI, we supplement the basic HH model by including the dynamics of $[K^+]_o$, the dynamics of $[O_2]_o$, and an additional excitatory synaptic current.

Dynamics of $[K^+]_o$.

To investigate how SBI occurs with the increased extracellular potassium levels, we modify *Eq. 5* by incorporating the dynamics of $[K^+]_o$ instead of using a constant value. It has been stated that the concentration of K^+ in the interstitial volume surrounding each cell is continuously updated relying on five types of currents, that is, K^+ current across the membrane (I_K), the neuronal Na^+-K^+ pump current (I_{pump}), glial Na^+-K^+ pump current ($I_{gliapump}$), glial buffering current (I_{glia}), and lateral diffusion current of K^+ between the extracellular space and bath solution (I_{diff}) (11). Based on such

recognition, Wei et al. (17) formulated the dynamics of $[K^+]_o$ to account for the spontaneous periodic seizure events, that is,

$$\frac{d[K^+]_o}{dt} = \gamma\beta I_K - 2\beta I_{pump} - I_{diff} - I_{glia} - 2I_{gliapump}. \quad (8)$$

In this paper, we aim at giving an interpretation for the occurrence of SBI by applying the same way to characterize the variation of $[K^+]_o$. Here, γ is a unit conversion factor that converts the current density to rate-of-change of concentration, and β is a dimensionless factor which represents the ratio of the intracellular volume to the extracellular volume.

Dynamics of $[O_2]_o$.

To investigate how SBI occurs with the decreased oxygen levels, we add the dynamical equation of $[O_2]_o$ in the original HH model. From the procedure of the oxidative phosphorylation, we know that O_2 is able to generate ATP that is mainly consumed by the activity of the neuronal and glial pumps (17). In addition, it has been stated that the supply of O_2 is mainly governed by the bath solution in in vitro experiments or by the microvasculature in vivo (i.e., $[O_2]_{bath}$) (17). Based on such points, the dynamics of $[O_2]_o$ can be characterized by the following linear differential equation (17):

$$\frac{d[O_2]_o}{dt} = -\alpha\lambda(I_{pump} + I_{gliapump}) + \epsilon_0([O_2]_{bath} - [O_2]_o), \quad (9)$$

where the left side $\frac{d[O_2]_o}{dt}$ represents the rate of oxygen (i.e., $[O_2]_{rate}$). The first term on the right side represents the oxygen consumption due to the neuronal pump and glial pump, and the second term represents the oxygen supply due to the bath solution. Parameter α is a conversion factor converting pump current to oxygen concentration change, and ϵ_0 is the diffusion rate. In this paper, we incorporate *Eq. 9* into HH model.

Formulation of excitotoxicity.

Excitotoxicity is the pathological process by which neurons are damaged and killed by overactivation of receptors for the excitatory neurotransmitter glutamate, including NMDA and AMPA receptors. Therefore, to a certain extent, the NMDA/AMPA receptor-mediated synaptic current can be used as a proxy for excitotoxicity. For simplicity, we neglect the type of excitatory receptors and directly apply the excitatory synaptic current (I_{exc}) to model excitotoxicity, and add it into the original membrane potential *Eq. 1* in HH model. The added excitatory current is formulated by

$$I_{exc} = -g_{excite}(t)(V - E_{excite}), \quad (10)$$

where g_{excite} denotes the time-dependent excitatory conductance (37). According to the work of Destexhe et al. (38), we model the source of synaptic conductance as a large number of weak synaptic inputs using a diffusion approximation, that is,

$$\frac{dg_{excite}}{dt} = -\frac{1}{\tau_{excite}}(g_{excite} - g_{mean}) + \sqrt{D_{excite}}\zeta_{excite}. \quad (10a)$$

Here, τ_{excite} is the time constant, ζ_{excite} is the White noise process, D_{excite} is the diffusion coefficient of the noise process, and E_{excite} is the corresponding reversal potential.

Mathematical formulation of SBIM.

In this part, we first clarify the formulation of reversal potentials E_{Na}, E_K, and E_{Cl}, which are critical in the mathematical modeling of SBIM. From *Eqs. 5–7*, it is obvious that the reversal potentials depend on the ion concentrations. Hence, we give the calculation of each ion concentration in what follows. Since the flow of K^+ out of the cell is assumed to be compensated by the flow of Na^+ into the cell, we apply the way described by Cressman et al. (11) to calculate $[K^+]_i$ as

$$[K^+]_i = [K^+]_{i,rest} + \left([Na^+]_{i,rest} - [Na^+]_i\right). \quad (11)$$

Here, $[K^+]_{i,rest}$ and $[Na^+]_{i,rest}$ represent the normal resting values of $[K^+]_i$ and $[Na^+]_i$. Moreover, $[Na^+]_i$ and $[Na^+]_o$ are calculated on the basis of the work by Wei et al. (11, 17, 39), that is,

$$\frac{d[Na^+]_i}{dt} = -\gamma I_{Na} - 3I_{pump}, \quad (12)$$

$$[Na^+]_o = [Na^+]_{o,rest} - \beta([Na^+]_i - [Na^+]_{i,rest}). \quad (13)$$

Here, $[Na^+]_{o,rest}$ is the $[Na^+]_o$ under normal resting conditions for a mammalian neuron (11). As for $[Cl^-]_i$ and $[Cl^-]_o$, we assume that they are fixed at 6 mM and 130 mM, respectively.

Next, we formulate four forms of currents I_{pump}, I_{glia}, $I_{gliapump}$, and I_{diff}, which play important roles on the dynamics of $[K^+]_o$ and $[O_2]_o$ in *Eqs. 8* and *9*. In this work, we apply the formulations in Ref. 11, that is,

$$I_{pump} = \frac{\rho}{1 + [\exp(25 - [Na^+]_i)/3]} \times \frac{1}{1 + \exp(5.5 - [K^+]_o)}, \quad (14)$$

$$I_{glia} = \frac{G_{glia}}{1 + \exp\left[\frac{(18 - [K^+]_o)}{2.5}\right]}, \quad (15)$$

$$I_{gliapump} = \frac{1}{3}\frac{\rho}{1 + [\exp(25 - [Na^+]_i)/3]} \times \frac{1}{1 + \exp(5.5 - [K^+]_o)}, \quad (16)$$

$$I_{diff} = \epsilon_k([K^+]_o - [K^+]_{bath}). \quad (17)$$

In *Eqs. 14–17*, parameter G_{glia} is the glia uptake strength; ρ is the pump/glia pump strength satisfying $\rho = \frac{\rho_{max}}{1 + \exp\left[\frac{(20 - [O_2]_o)}{3}\right]}$, where ρ_{max} is the maximal strength of Na^+-K^+ pump in the fully oxygenated state; $[K^+]_{bath}$ is the potassium concentration in the largest nearby reservoir corresponding to either the bath solution in a slice preparation, or the vasculature in the intact brain. The parameter ϵ_k is the potassium diffusion rate. It represents the diffusion of K^+ from the local extracellular microenvironment to blood vessels/bath solution, where K^+ is transported through astrocytic glial cells and released from their endfeet into blood vessels (40). Meanwhile, it is reported that ion transport between glial cells and blood vessels is dependent upon active transport

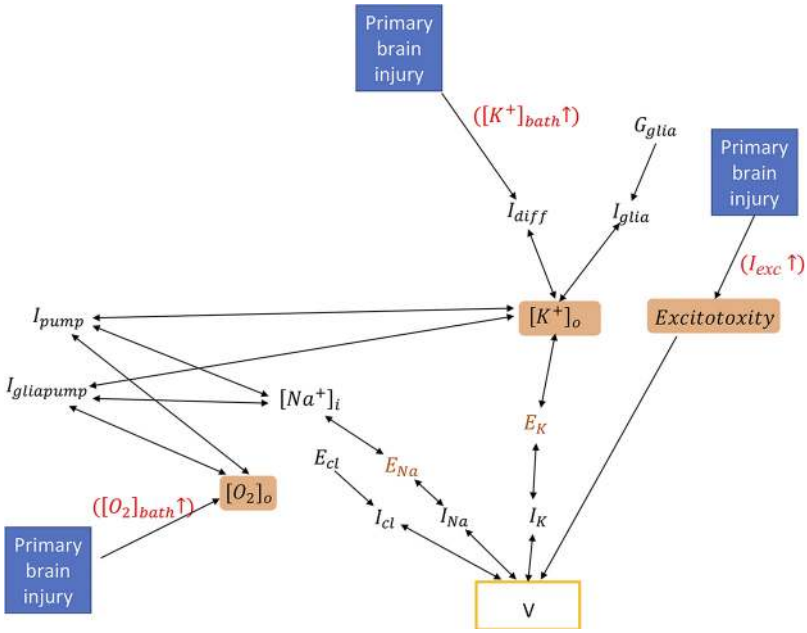

Figure 2. Relationship among all variables in SBIM. E_{Cl}, reversal potential of Cl^-; E_K, reversal potential of K^+; E_{Na}, reversal potential of Na^+; G_{glia}, glia uptake strength; I_{Cl}, chloride leak current; I_{diff}, lateral diffusion current of K^+ between the extracellular space and bath solution; I_{glia}, glial buffering current; I_{exc}, excitatory synaptic current; $I_{gliapump}$, glial Na^+–K^+ pump current; I_K, potassium current; I_{Na}, sodium current; I_{pump}, neuronal Na^+–K^+ pump current; $[K^+]$, K^+ concentration; $[K^+]_o$, extracellular K^+ concentration; $[Na^+]_i$, intracellular Na^+ concentration; $[O_2]$, oxygen concentration; $[O_2]_o$, extracellular oxygen concentration; SBIM, secondary brain injury model; V, membrane potential.

through the Na^+/K^+ pump (41), which in turn is related to the oxygen concentration. Therefore, we formulate ϵ_k as a sigmoid function of O_2 level rather than a constant according to the work of Wei et al. (14), that is,

$$\epsilon_k = \frac{\epsilon_{k,max}}{1 + \exp\left(-\frac{[O_2]_{bath}-5}{5}\right)}, \quad (18)$$

where $\epsilon_{k,max}$ is the maximal potassium diffusion rate.

In general, the mathematical equations of SBIM are obtained by combining HH model with the formulation of SBI mechanisms shown in *Eqs. 8–18*. The final model output is the membrane potential V, which is the solution of the following dynamical equation

$$\frac{dV}{dt} = \frac{1}{C}(I_e - I_{Na} - I_K - I_{Cl} + I_{exc}). \quad (19)$$

Figure 2 provides a visualization of the dependency relationship among all variables in SBIM. Here, a one-way arrow ($A \rightarrow B$) signifies that variable A affects the dynamics of variable B, and a two-way arrow ($A \leftrightarrow B$) means that there exists a bidirectional interaction between A and B. In our proposed model, the nominal values of all parameters are listed in Table 1 (referenced in Ref. 17).

EXPERIMENTS AND RESULTS

Experimental Approach

Seizures, particularly nonconvulsive seizures, are commonly found on EEG following acute brain injury. Wei et al. (17) found that oxygen utilization increases during and following seizures, requiring ion pumps to expend energy to restore ion gradients, and this, in combination with the significant time required for oxygen to diffuse from bath solution into the extracellular space, leads to tissue hypoxia. Witsch et al. (5) found in patients with SAH that this effect on brain tissue oxygenation was dependent on discharge frequency within seizures and periodic discharges (higher-frequency discharges causing more metabolic stress that is not compensated for adequately after acute brain injury compared with lower-frequency discharges). To explore the relationship among seizures, tissue hypoxia, and brain injury, we define two indices as follows:

First, we define the "hypoxia index (HI)" to represent the cumulative burden of hypoxia as

$$\mathrm{HI} = \int_0^T \Theta(\mathrm{Thr} - [O_2]_o)(\mathrm{Thr} - [O_2]_o)dt. \quad (20)$$

Table 1. *Nominal values of all parameters in SBIM*

Parameter	Values, Units	Parameter	Values, Units	Parameter	Values, Units
G_{Na}	30 mS/cm^2	ρ_{max}	1.25 mM/s	γ	0.0445 mM/s/μA/cm^2
G_{NaL}	0.01750 mS/cm^2	C	1 μF/cm^2	$[O_2]_{bath}$	32 mg/L
G_K	25 mS/cm^2	α	5.3 g/mol	$[K^+]_{bath}$	4 mM
G_{KL}	0.05 mS/cm^2	λ	1	E_{excite}	0 mV
G_{CLL}	0.05 mS/cm^2	ϵ_0	0.17 s^{-1}	$[Na^+]_{i,rest}$	18 mM
E_{CL}	–81.9386 mV	G_{glia}	8 mM/s	$[K^+]_{i,rest}$	140 mM
β	7	$\epsilon_{k_{max}}$	0.33 s^{-1}	$[Na^+]_{o,rest}$	144 mM
Thr	24 mg/L	Thr_1	–88 mV	Thr_2	60 mV
g_{mean}	0.005 mS/cm^2	D_{excite}	1	τ_{excite}	3.3 ms

SBIM, secondary brain injury model. See text for definitions of model parameters.

Here, HI is taken as a measure of ongoing brain injury (42), as well as a proxy for the severity and extent of SBI, where Thr is named as the "brain injury threshold," $\Theta(\cdot)$ is the Heaviside function, and T is the duration of the experiment. Obviously, the higher the value of HI is, the more severe SBI will be.

Next, we define the "epileptiform activity intensity (EI)" as

$$\mathrm{EI} = \frac{\text{time with epileptiform discharges}}{\text{total EEG time}} \times \frac{\text{no. of epileptiform discharges}}{\text{time with epileptiform discharges}}(\mathrm{Hz}), \qquad (21)$$

to measure the intensity of epileptiform activity(i.e., seizures or PDs). The first term of EI represents the epileptiform burden, which is the proportion of time occupied by seizures or PDs during a period of EEG recording. The second term represents discharge frequency [i.e., rate of epileptiform discharges (Hz)], which is the number of epileptiform discharges per second within a seizure or a train of PDs. In this work, we take EI as a measure of the severity of seizures or PDs, as well as the propensity to induce metabolic crisis by seizures or PDs. Obviously, EI becomes larger with the increase of epileptiform burden and discharge frequency.

Seen from Fig. 2, we found that E_K and E_{Na} are in the key position and exert important effects on the variables in SBIM. Therefore, we also define two indices,

$$V_{E_K} = \int_0^T \Theta(E_K - \mathrm{Thr}_1)(E_K - \mathrm{Thr}_1)dt$$

and

$$V_{E_{Na}} = \int_0^T \Theta(\mathrm{Thr}_2 - E_{Na})(\mathrm{Thr}_2 - E_{Na})dt, \qquad (22)$$

to geometrically measure the area between the E_K versus time curve and a threshold value $E_K = \mathrm{Thr}_1$, and the area between the E_{Na} versus time curve and a threshold value $E_{Na} = \mathrm{Thr}_2$. It is obvious that the lower the absolute values of E_K and E_{Na} are, the larger the values of V_{E_K} and $V_{E_{Na}}$ will be.

In the following, we apply the proposed neural computational model SBIM to investigate how three key factors ($[O_2]_o$, $[K^+]_o$, I_{exc}) affect seizures and SBI with the defined measures HI, EI, V_{E_K}, and $V_{E_{Na}}$ We note that our analysis focuses on acute manipulations and their acute consequences, such as would occur during a hospitalization, rather than long-term changes such as might occur in the weeks or months following an acute injury. Meanwhile, the explanations for several important observations obtained in the experiments will be also clarified by the model SBIM. To realize our objective, three key model parameters: $[K^+]_{bath}$, $[O_2]_{bath}$, and g_{mean} are varied in our experiments. Here, the range of $[K^+]_{bath}$ is set to be [4 mM, 10 mM], as in Ref. 43. The range of $[O_2]_{bath}$ is set to be the same values used in the work of Wei et al. (17) (i.e., [15 mg/L, 32 mg/L]) in investigating oxygen and seizure dynamics. The baseline value of g_{mean} is set to be 0.005, which agrees with the range [0.005, 0.0375] given to simulate synaptic background activity in the work by Destexhe et al. (38). In addition, we set brain injury threshold Thr to be 24 mg/L. We have verified that if Thr is set to a value from 20 mg/L to 28 mg/L, similar experimental results are obtained. The thresholds Thr_1 and Thr_2 are set to be −88 mV and 60 mV, respectively, according to the reversal potential constant values in mammalian neurons. All simulations were performed using Matlab (MathWorks, Natick, MA) software, and the fourth-order Runge–Kutta method was used for integrating all differential equations. For *Eq. 10a*, a noise realization was added at each step.

Experimental Results

Increased $[K^+]_o$ induces SBI.

We simulate spillage of K^+ into the extracellular space ($[K^+]_o$)from damaged neurons after PBI, by varying the model parameter $[K^+]_{bath}$ from its normal value of 4 mM up to a higher value 10 mM and calculate the resulting measures of SBI: HI, EI, V_{E_K}, and $V_{E_{Na}}$. As we increased $[K^+]_{bath}$, local available $[K^+]_o$ increases. Model behaviors for three values of $[K^+]_{bath}$ = 4, 6, 9 mM are shown in Fig. 3, *A–C*, respectively. For these experiments, all parameters, except $[K^+]_{bath}$, are set to their nominal values listed in Table 1. We also neglect the influence of excitatory neurotransmitters, by setting I_{exc} to 0. We define the model output as showing a "seizure" where there is a cluster of discharges.

For the membrane potential trace V given by the model, we see that with increasing levels, the number of seizures increases [no seizure for $[K^+]_{bath}$ = 4 mM (Fig. 3*A*), 1 seizure for $[K^+]_{bath}$ = 6 mM (Fig. 3*B*), and 4 seizures for $[K^+]_{bath}$ = 9 mM (Fig. 3*C*)]. Simultaneously, the epileptiform burden (fraction of time with seizures) increases from 0, to 0.11, to 0.61. Also, the frequency of discharges within the seizure increases from 0 Hz to 121.4 Hz, and then to 432.7 Hz. Overall, the increasing epileptiform burden and the discharge frequency increase the intensity of epileptiform activity, EI. For the $[O_2]_o$ profile, we see that, with increased $[K^+]_{bath}$, more O_2 is needed to support the more intense spiking activity, which results in a higher burden of hypoxia (i.e., larger gray area for $[O_2]_o$ under the threshold Thr). In addition, increasing $[K^+]_{bath}$ leads to a higher E_K and thus a larger gray area for E_K above the threshold Thr_1, and a lower E_{Na} and thus a larger gray area for E_{Na} under the threshold Thr_2.

The overall relationship between $[K^+]_{bath}$ and SBI is demonstrated in Fig. 4. We found that EI increases with increasing levels of $[K^+]_{bath}$ resulting from PBI, and the severity and extent of SBI (i.e., HI) increases with increasing EI, where the color bar represents the value of HI (Fig. 4*A*).This implies that more severe brain injury, associated with increased $[K^+]_o$, is associated with more intense seizures. This is consistent with the physiological observations in the literature. We also found that V_{E_K} and $V_{E_{Na}}$ increase with increasing EI; color bars represent the value of V_{E_K} and $V_{E_{Na}}$, respectively (Fig. 4, *B* and *C*). This might imply that the transition from PBI to SBI resulting from the increase of $[K^+]_o$ is accompanied by increasing E_K and decreasing E_{Na}.

Excitotoxicity induces SBI.

We next simulate excitation of neural tissue due to excessive excitatory neurotransmission after PBI, by injecting an external excitatory synaptic current I_{exc} into the model, which is taken as a variable satisfying the dynamics of excitatory conductance (g_{exc}) and membrane potential (V). As we decrease

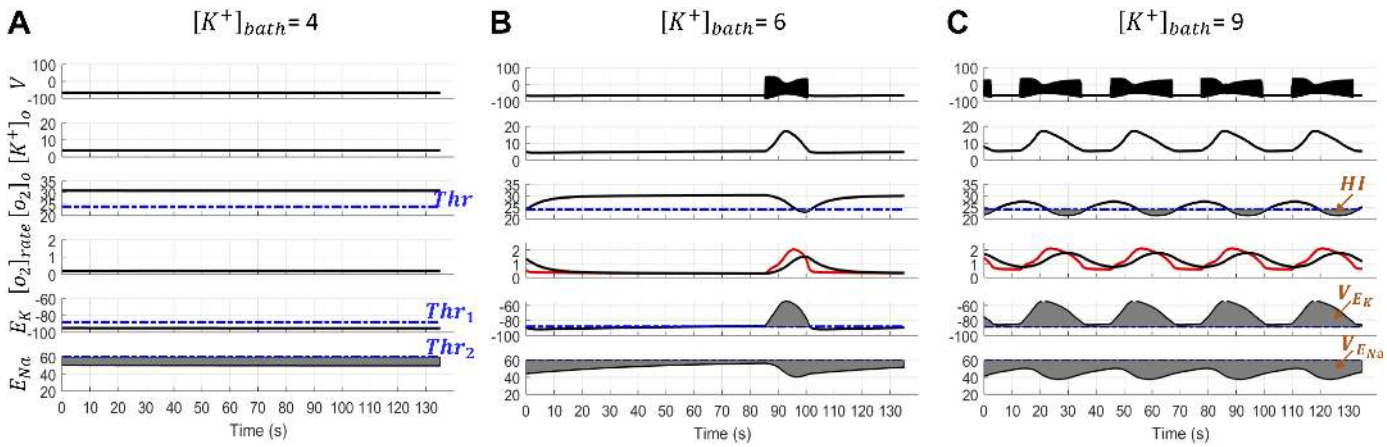

Figure 3. Epileptiform activity intensity increases with ambient potassium levels. Plots show model outputs over time, including the membrane potential *V*; extracellular K^+ concentration ($[K^+]_o$); extracellular oxygen concentration ($[O_2]_o$); rate of oxygen consumption ($[O_2]_{rate}$) due to pump activity (red curve), and rate of oxygen replenishment by diffusion from bath solution (black curve); reversal potentials of K^+ (E_K) and Na^+ (E_{Na}). These are shown for three levels of bath potassium: $[K^+]_{bath}$ = 4 mM (*A*), $[K^+]_{bath}$ = 6 mM (*B*), and $[K^+]_{bath}$ = 9 mM (*C*). The dotted lines in the plots for $[O_2]_o$, E_K, and E_{Na} are the corresponding thresholds Thr, Thr_1, and Thr_2. The area of the gray regions represent hypoxia index (HI), V_{E_K}, and $V_{E_{Na}}$ defined in *Eqs. 20* and *22*, respectively. V_{E_K}, quantities of reversal potential of K^+; $V_{E_{Na}}$, quantities of reversal potential of Na^+.

the mean value of g_{exc} (i.e., g_{mean}), available I_{exc} increases, indicating more excitotoxity.

We experimentally vary g_{mean} in the model from 1 to 0.005. The simulated model behavior for three values of g_{mean} = 1, 0.47, and 0. 02 are shown in Fig. 5, in which all the other parameters are set to be their nominal values listed in Table 1, except $[K^+]_{bath}$. We consider two cases for $[K^+]_{bath}$: its normal value (4 mM, Fig. 5, *A–C*) and a higher value (8.5 mM, Fig. 5, *D–F*). We see that there is no epileptiform activity when $[K^+]_{bath}$ is normal, although g_{mean} is decreased (Fig. 5, *A–C*). However, when $[K^+]_{bath}$ is higher, decreasing g_{mean} leads to increased numbers of seizures [no seizure for g_{mean} = 1 (Fig. 5*D*), 3 seizures for g_{mean} = 0.47 (Fig. 5*E*), and 4 seizures for g_{mean} = 0.02 (Fig. 5*F*)]. Meanwhile, the epileptiform burden and frequency of discharges within the seizures increase simultaneously, which results in increasing seizure intensity. Similarly, more hypoxia occurs with decreased g_{mean} and increased intensity of seizures (third row in Fig. 5, *D–F*). Also, decreasing g_{mean} leads to a higher E_K (fifth row in Fig. 5, *D–F*), and to a lower E_{Na} (sixth row in Fig. 5, *D–F*).

The overall relationship between excitotoxicity and SBI is shown in Fig. 6. We found that EI increases with increasing levels of excitotoxity (i.e., decreasing g_{mean}) resulting from PBI, and severity of SBI (i.e., HI) in turn increases with increasing EI (Fig. 6*A*).This implies that more severe brain injury, associated with increased excitotoxity, is also associated with more intense seizures. Similarly, we observe that V_{E_K} and $V_{E_{Na}}$ increase with increasing EI (Fig. 6, *B* and *C*). This might suggest that the transition from PBI to SBI resulting from excitotoxicity is also accompanied by increasing E_K and decreasing E_{Na}.

Decreased $[O_2]_o$ and SBI.

We next simulate reduced oxidative metabolism after PBI, by varying the model parameter $[O_2]_{bath}$ from its normal value 32 mg/L to a lower value 15 mg/L. Simulated model behaviors, with $[O_2]_{bath}$ equals to 32 mg/L, 26 mg/L, and 22 mg/L, are shown in Fig. 7. Other parameters are set to be their nominal values listed in Table 1, except $[K^+]_{bath}$, which is set to its normal value (4 mM, Fig. 7, *A–C*) and to a

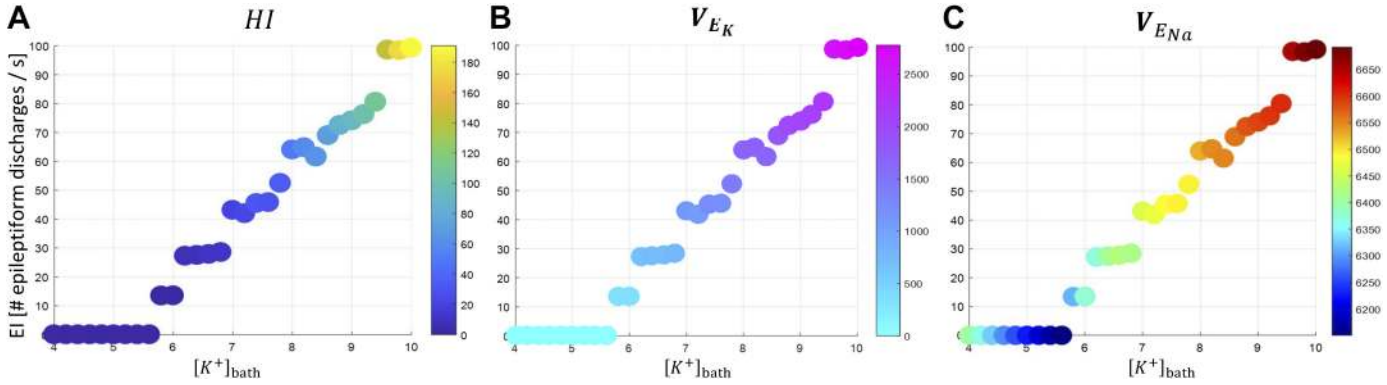

Figure 4. Relationships between bath potassium levels and SBI. *A*: relationship among $[K^+]_{bath}$, epileptiform activity intensity (EI), and hypoxia index (HI). The color bar indicates the value of the brain injury, HI. *B*: relationship among $[K^+]_{bath}$, EI, and V_{E_K}. The color bar indicates the value of V_{E_K}. C: relationship among $[K^+]_{bath}$, EI, and $V_{E_{Na}}$. The color bar indicates the value of $V_{E_{Na}}$. SBI, secondary brain injury; V_{E_K}, quantities of reversal potential of K^+; $V_{E_{Na}}$, quantities of reversal potential of Na^+.

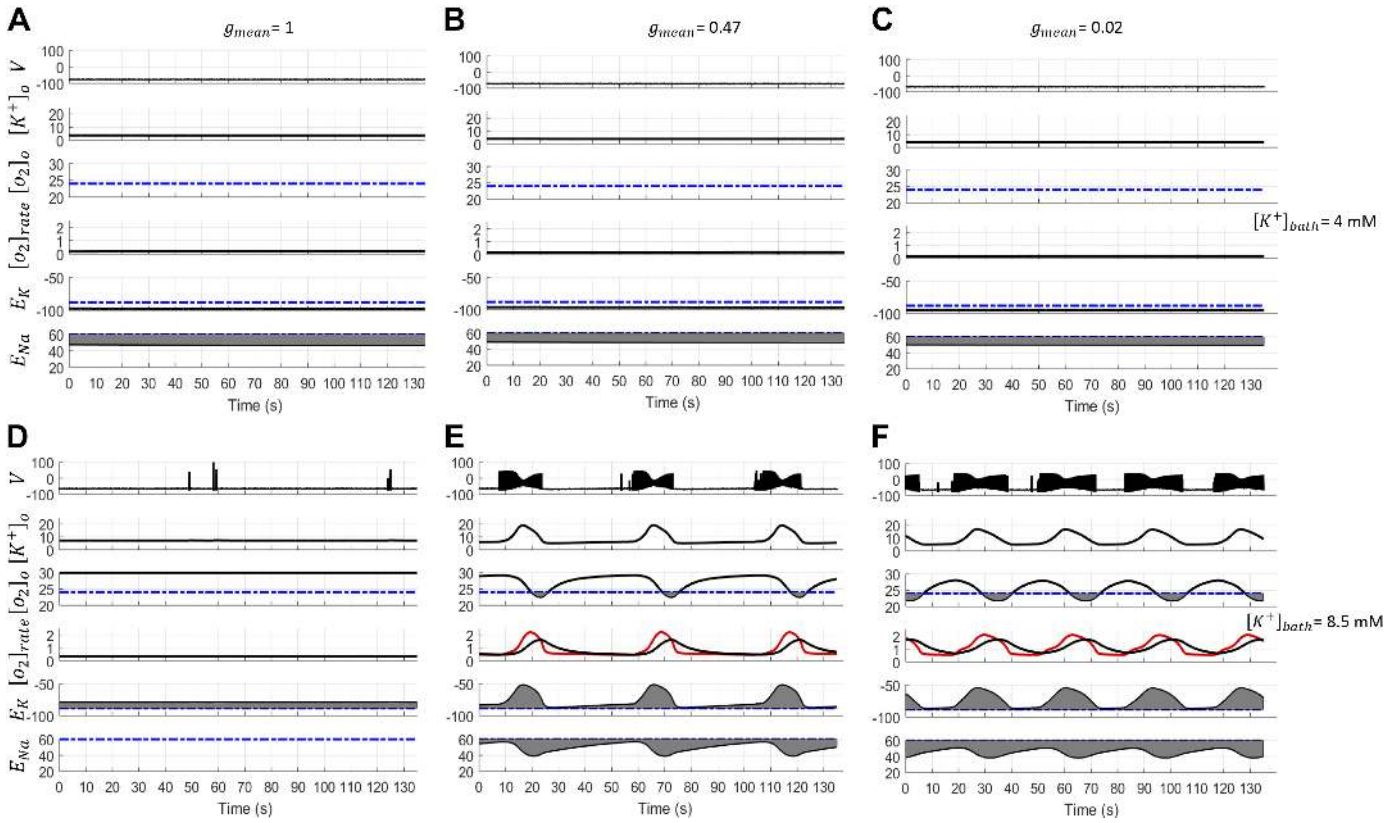

Figure 5. Epileptiform activity intensity increases with increasing levels of excitotoxicity, when bath potassium levels are elevated. Plots show the membrane potential *V*, extracellular K^+ concentration ($[K^+]_o$), extracellular O_2 concentration ($[O_2]_o$), O_2 consumption rate ($[O_2]_{rate}$), and reversal potentials of K^+ (E_K) and Na^+ (E_{Na}) for g_{mean} = 1 (*A* and *D*), g_{mean} = 0.47 (*B* and *E*), g_{mean} = 0.02 (*C* and *F*), $[K^+]_{bath}$ = 4 for (*A*–*C*), and $[K^+]_{bath}$ = 8.5 for (*D*–*F*). g_{mean}, Mean value of excitatory conductance.

higher value (8.5 mM, Fig. 7, *D*–*F*). Under the condition of normal $[K^+]_{bath}$, following Wei et al. (17), an external input is applied (i.e., I_e = 0.5) to mimic a slightly excitable state. For these experiments, we neglect the influence of increased excitatory neurotransmission by setting I_{exc} to be 0.

We see that when $[K^+]_{bath}$ is normal, the model exhibits tonic firing activity at $[O_2]_{bath}$ = 32 mg/L (Fig. 7*A*). Seizures appear when $[O_2]_{bath}$ decreases to 26 mg/L (Fig. 7*B*), and then disappear when $[O_2]_{bath}$ is further decreased to 22 mg/L (Fig. 7*C*). Further experiments (not shown) show that seizure events occur within a narrow range of $[O_2]_{bath}$ (22–27 mg/L) under normal bath potassium concentrations. When $[K^+]_{bath}$ is increased to 8.5 mM, seizures occur for a larger range of $[O_2]_{bath}$, although seizures occur less often and are briefer with decreasing values of $[O_2]_{bath}$. This pattern is seen in Fig. 7, *D*–*F*, where the model exhibits periodic seizures when $[O_2]_{bath}$ equals 32 mg/L, 26 mg/L, and 22 mg/L, respectively, with corresponding EI values of 66.4, 63.5, and 59.1. And the more

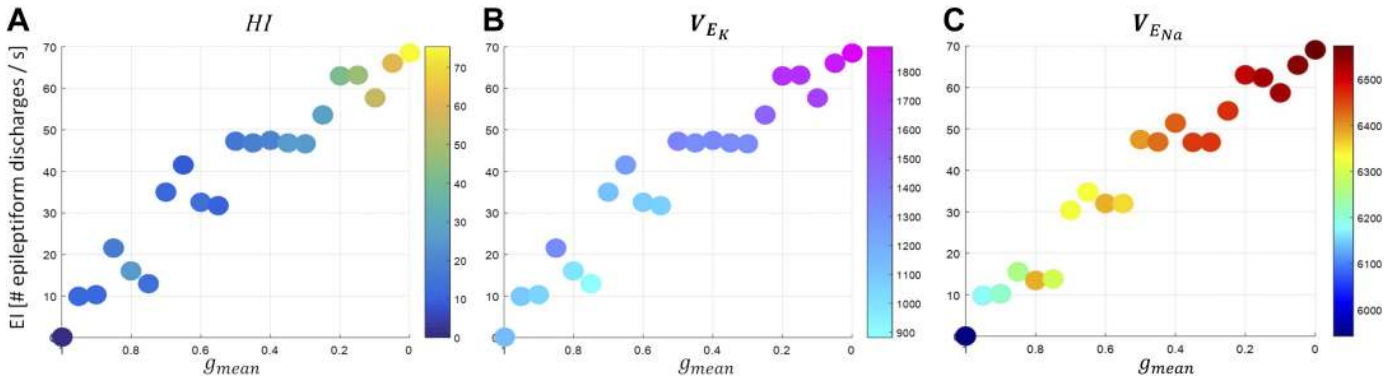

Figure 6. Relationships between excitotoxicity and SBI. *A*: relationship among g_{mean}, frequency (epileptiform activity intensity, EI), and hypoxia index (HI). *B*: relationship among g_{mean}, EI, and V_{E_K}. *C*: relationship between g_{mean}, EI, and $V_{E_{Na}}$. EI, epileptiform activity intensity; g_{mean}, linear function of epileptiform activity intensity; HI, hypoxia index; SBI, secondary brain injury; V_{E_K}, quantities of reversal potential of K^+; $V_{E_{Na}}$, quantities of reversal potential of Na^+.

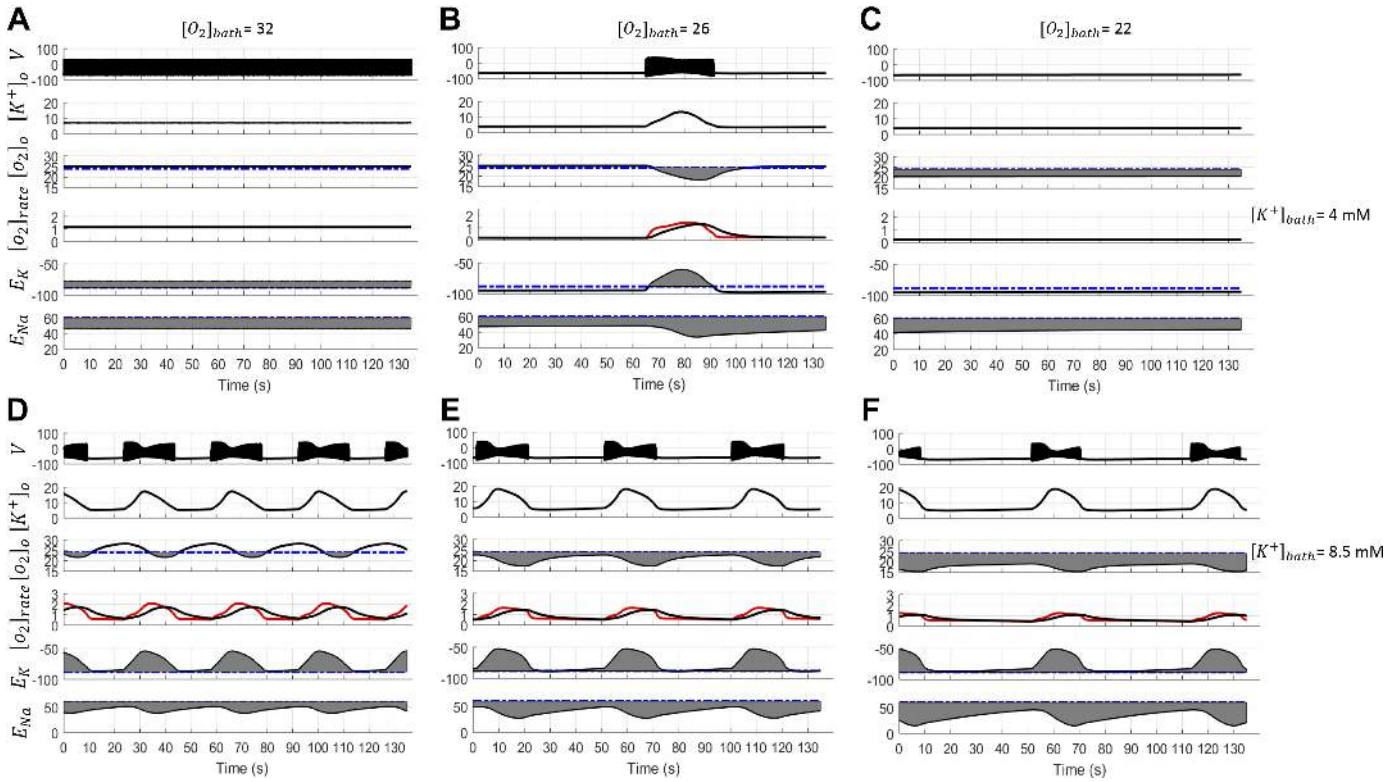

Figure 7. Seizures occur within a narrow range of oxygen levels. This range depends on bath potassium concentration. Epileptiform activity intensity decreases with decreasing oxygen levels. Plots show the membrane potential *V*, extracellular K^+ concentration ($[K^+]_o$), extracellular O_2 concentration ($[O_2]_o$), O_2 consumption rate ($[O_2]_{rate}$), and reversal potentials of K^+ and Na^+ for $[O_2]_{bath}$ = 32 mg/L (*A* and *D*), $[O_2]_{bath}$ = 26 mg/L (*B* and *E*), $[O_2]_{bath}$ = 22 mg/L (*C* and *F*). $[K^+]_{bath}$ = 4 for (*A*–*C*), and $[K^+]_{bath}$ = 8.5 for (*D*–*F*). E_K, reversal potential of K^+; E_{Na}, reversal potential of Na^+.

hypoxia occurs as increased intensity of seizures (i.e., the larger the gray area of $[O_2]_o$ under the threshold). The overall relationship between $[O_2]_{bath}$ and SBI is described in Fig. 8. We find that as $[O_2]_{bath}$ decreases resulting from PBI, the EI decreases (seizures become briefer and less frequent), and severity of SBI (i.e., HI) increases (Fig. 8*A*). In addition, V_{E_K} decreases with decreasing EI, and conversely, $V_{E_{Na}}$ increases with decreasing EI (Fig. 8, *B* and *C*). This might imply that the transition from PBI to SBI resulting from decreased O_2 level is accompanied by decreasing E_K and E_{Na}.

We also see that when hypoxia becomes severe, the model exhibits burst suppression-like activity. Figure 9 illustrates this model behavior with $[O_2]_{bath}$ =15. To clarify the change of neuron behaviors due to varying $[O_2]_{bath}$, we perform analysis of these dynamical bifurcations as a function of $[K^+]_o$ and $[Na^+]_i$. The bifurcation diagram in Fig. 9*B* describes neuronal asymptotic behaviors associated with different fixed values of $[K^+]_o$ and $[Na^+]_i$, where the "SN" denotes the saddle-node bifurcation curve and "HB" denotes the Hopf bifurcation curve. To the left of the SN curve, the neuron approaches a stable equilibrium resting state. The neuron spikes regularly between SN and HB

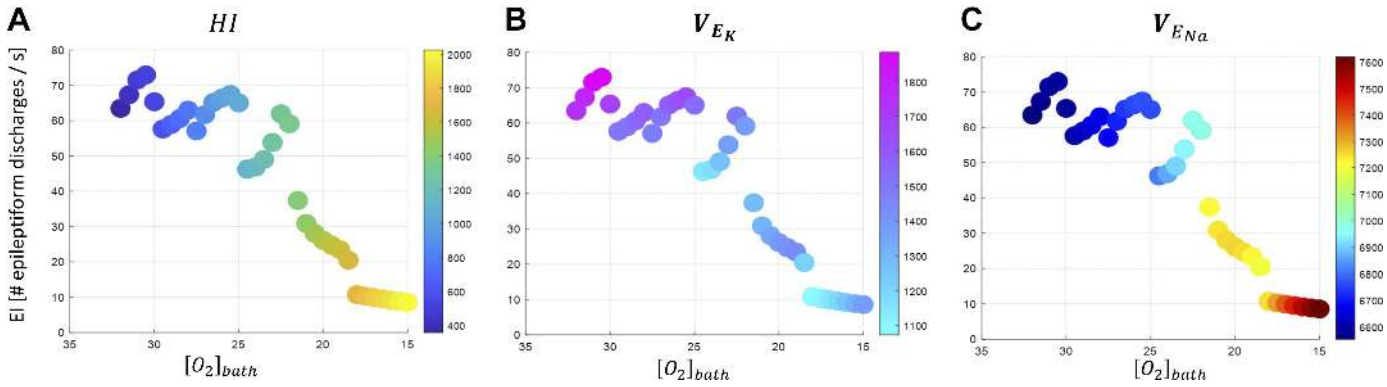

Figure 8. Relationships between hypoxia and SBI. *A*: relationship between $[O_2]_{bath}$, EI, and HI. *B*: relationship between $[O_2]_{bath}$, EI, and E_K. *C*: relationship among $[O_2]_{bath}$, EI, and E_{Na}. EI, epileptiform activity intensity; E_K, reversal potential of K^+; E_{Na}, reversal potential of Na^+; HI, hypoxia index; SBI, secondary brain injury; V_{E_K}, quantities of reversal potential of K^+; $V_{E_{Na}}$, quantities of reversal potential of Na^+.

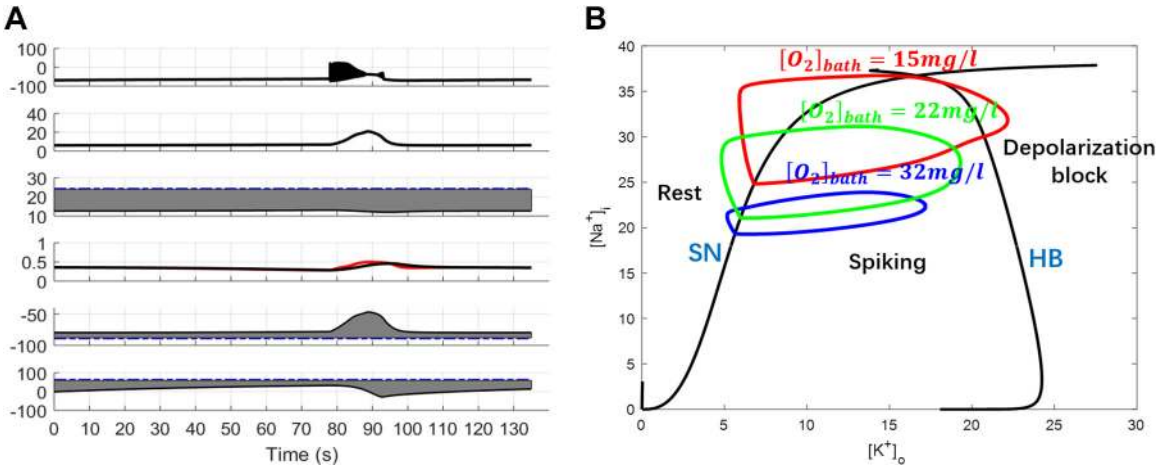

Figure 9. *A*: severe hypoxia leads to burst suppression-like activity. In brain injury resulting in severe hypoxia-ischemia, the model produces not seizures, but instead a "burst suppression" pattern, and ultimately electrical silence. In the example shown here, neuronal activity transitions from rest, to spiking, to depolarization block, then a quiescent state. *B*: bifurcation analysis with ion concentration dynamics when $[O_2]_{bath}$ vary. The loops are traversed in a counterclockwise manner, with $[O_2]_{bath}$ = 32 mg/L (blue), 22 mg/L (green), and 15 mg/L (red), respectively. $[K^+]_o$, extracellular K^+ concentration. HB, Hopf bifurcation curve; SN, saddle-node bifurcation curve.

curves. To the right of the HB curve, the cell is attracted to a stable equilibrium depolarization block state (39). We have overlaid trajectories of ion dynamics onto the bifurcation diagram for three levels of $[O_2]_{bath}$: 32, 22, 15 mg/L. We see that for $[O_2]_{bath}$ = 32 mg/L and 22 mg/L, the loops do not cross the HB curve, and only traverse between resting and spiking in a counterclockwise manner. In these cases, the cell exhibits spontaneous periodic seizures alternating with a resting state. When $[O_2]_{bath}$ = 15 mg/L, the loop grows large enough to cross the HB curve, and then return from depolarization block to the rest state and does not cross the HB curve, and therefore involves no spikes. In this case, the neuron behavior traverses from rest, to spiking, to depolarization block, followed by a quiescent state. This reflects the limited ability of pump activity to restore ion gradients, causing the neuron to remain inactivated. This is consistent with the observation (44) that severe anoxic brain injury results not in seizures, but instead in "burst suppression" and ultimately electrical inactivity.

In summary, the results of the foregoing computer simulations provide explanations for how *1*) brain injury can lead to seizure activity; *2*) seizure activity can exacerbate tissue hypoxia; *3*) more severe brain injury can lead to more intense seizure activity.

Summary of our model for the MSDMH.

Here, we summarize the results of our computational experiments by tracing three underlying paths for how PBI can evolve into SBI (Fig. 10). In the course of this discussion, we provide additional experiments to illustrate how the main results interact.

The first pathway relates to extracellular potassium. In the experimental results of Fig. 3, we found that increased $[K^+]_o$, simulated by elevated $[K^+]_{bath}$ resulting from PBI, promotes seizures. This is consistent with observations by Raimondo et al. (13), where it is pointed out that epileptogenic changes result in enhanced extracellular K^+ accumulation

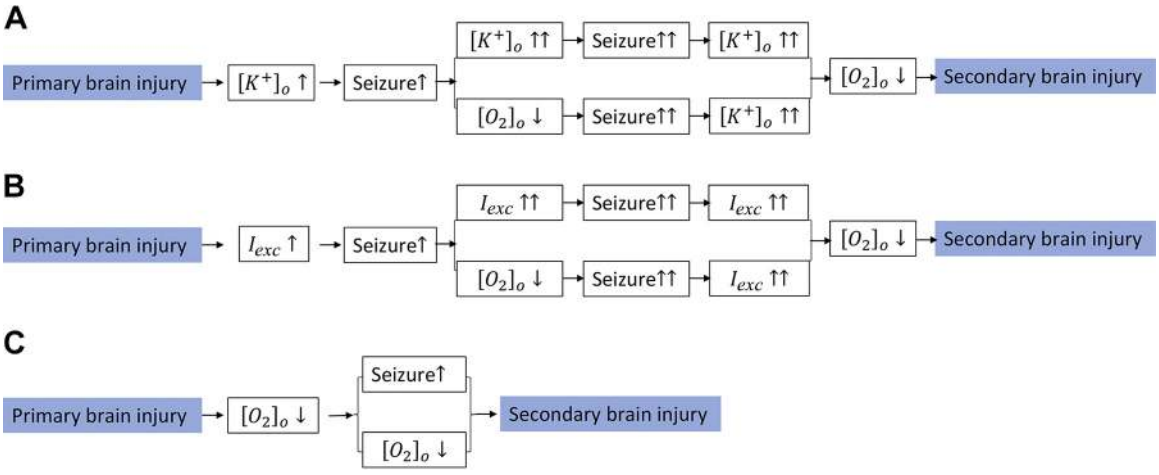

Figure 10. The three possible models for how primary brain injury (PBI), exacerbated by increased extracellular potassium (*A*), excitotoxicity (*B*), and decreased oxygen level (*C*), evolve to secondary brain injury (SBI). I_{exc}, excitatory synaptic current; $[K^+]_o$, extracellular potassium concentration; $[O_2]_o$, extracellular oxygen concentration.

during physiological activity, which triggers onset of seizures and a further increase in $[K^+]_o$. To model accumulation of $[K^+]_o$ induced by seizures, we set $[K^+]_{bath}$ as a variable related to EI, rather than a constant as in previous experiments. For simplicity, let us assume $[K^+]_{bath}$ is a linear function of EI, and $[K^+]_{bath}$ (EI) = $[K^+]_{bath,initial} + \alpha_1(EI - EI_{initial})$, where $[K^+]_{bath,initial}$ represents the initial value of $[K^+]_{bath}$, $EI_{initial}$ is the initial value of EI, and α_1 is a constant of proportionality (here, α_2 = 0.1). This simple model expresses the observation that, the higher the EI, the more extracellular potassium will be accumulated (i.e., the higher $[K^+]_{bath}$ or $[K^+]_o$ will be).

From this model, we can obtain one key mechanistic pathway for how PBI can evolve into SBI due to the increase of $[K^+]_o$, shown in Fig. 11. The initial value of $[K^+]_{bath}$ equals 6 mM due to primary injury. This promotes occurrence of seizures. Subsequently, on the one hand increased seizure activity decreases the level of extracellular O_2 because more oxygen is required to maintain activity of the Na^+-K^+-pump to restore ion gradients (shown by *1* in Fig. 11). On the other hand, seizure activity further enhances the amount of extracellular $[K^+]_o$ (shown by *2* in Fig. 11). Furthermore, the increase in $[K^+]_o$ and decrease in $[O_2]_o$ induce more intense seizure activity (EI) (shown by *3* in Fig. 11). In turn, $[K^+]_o$ levels are further increased (shown by *4* in Fig. 11). More pump activity is needed to restore ion gradients, which requires more oxygen consumption, causing $[O_2]_o$ to drop further (shown by *5* in Fig. 11). Together, these processes result in SBI. Based on this, the first possible route by which PBI evolves into SBI according to our model is summarized in Fig. 10*A*.

The second pathway relates to excitotoxicity. In the experiments shown in Fig. 5, we found that increasing I_{exc} due to PBI, simulated by reduced g_{mean}, promotes seizures. In addition, increased expression of neuronal glutamate transporters (EAAT3/EAAC1) in both rats and humans occurs with epileptic seizures (45). To model this worsening excitotoxicity induced by seizures, we set g_{mean} as a variable related to epileptiform activity intensity. For simplicity, we assume that g_{mean} is a linear function of EI, and g_{mean}(EI) = $g_{mean,initial} - \alpha_2(EI - EI_{initial})$, where $g_{mean,initial}$ represents the initial value of g_{mean}, and α_2 is a proportionality constant (here, α_2 = 0.03). This equation expresses the observation that, the higher the EI, the more excitotoxicity will be induced (i.e., the lower the g_{mean} or higher the I_{exc} will be). From this model we can obtain an integral mechanism pathway about how PBI evolves into SBI due to excitotoxicity, shown in Fig. 12. The initial value of g_{mean} = 0.9. Based on this, a second possible route by which PBI evolves into SBI is summarized in Fig. 10*B*.

The third pathway relates to tissue hypoxia. In the experiments shown in Fig. 7, we found that decreasing O_2 resulting from PBI promotes seizures, which we simulated by reduced $[O_2]_{bath}$. Furthermore, seizures promote activation of the Na^+-K^+-pump, leading to increased oxygen consumption, which decreases local tissue $[O_2]_o$. To simulate decreasing $[O_2]_o$ induced by seizures, we set $[O_2]_{bath}$ as a variable related to epileptiform activity intensity. For simplicity, we assume that $[O_2]_{bath}$ is a linear function of EI, $[O_2]_{bath}$ (EI) = $[O_2]_{bath,initial} - \alpha_3$ (EI − $EI_{initial}$), where $[O_2]_{bath,initial}$ is the initial value of $[O_2]_{bath}$, and α_3 is a proportionality constant (here, α_3 = 0.1). This model captures the observation that higher oxygen consumption is needed to support more intense epileptiform activity (i.e., the lower $[O_2]_{bath}$ or $[O_2]_o$ will be). The corresponding result is shown in Fig. 13. The initial value of $[O_2]_{bath}$ = 32. We summarize these results as the third route by which PBI can evolve into SBI in Fig. 10*C*. Here, decreasing O_2 due to primary brain injury promotes seizures, leading in turn to

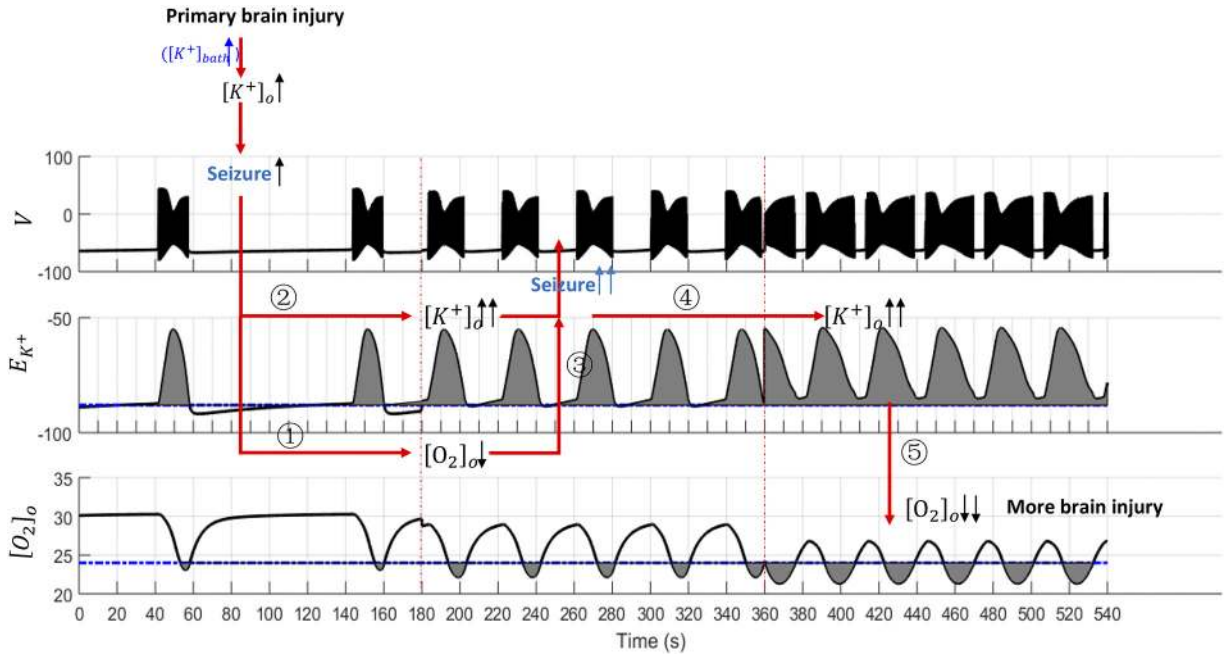

Figure 11. Increased potassium: first pathway for evolution of primary brain injury (PBI) into secondary brain injury (SBI). Dependence of model output (*V*), reversal potential of K^+, and O_2 concentration related to increased $[K^+]_o$ induced by PBI. These observations are summarized in Fig. 10*A*. E_{K^+}, reversal potential of K^+; $[K^+]_o$, extracellular potassium concentration; $[O_2]_o$, extracellular oxygen concentration.

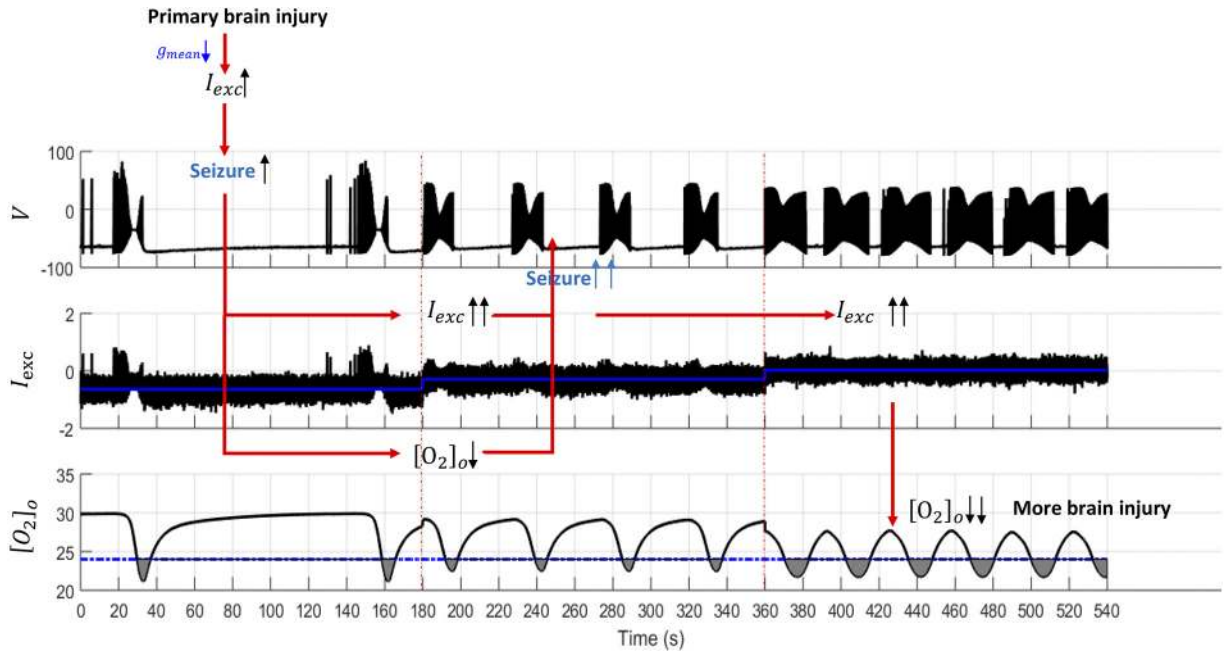

Figure 12. Increased excitotoxicity: second pathway for evolution of primary brain injury (PBI) into secondary brain injury (SBI). Model response to output (reversal potential of K^+ and O_2 concentration) in relation to increased excitotoxicity (I_{exc}) induced by PBI. These observations are summarized in Fig. 10*B*. g_{mean}, Mean value of excitatory conductance; $[O_2]_o$, extracellular oxygen concentration; *V*, membrane potential.

further decreases in oxygen levels. In this case, SBI will occur if there is insufficient supply of O_2.

DISCUSSION

In this work, we have built a mechanistic model that implements, at least in part, the metabolic supply demand mismatch hypothesis (MSDMH), which has been proposed to explain why patients with acute brain injury frequently develop seizure activity and secondary brain injury (SBI). According to the MSDMH, SBI arises from interactions among several factors, including compromised metabolic reserve, seizures and periodic discharges (PDs), ischemia, hypoxia, and possibly inflammation. These factors combine to induce a state of supply-demand mismatch, or metabolic crisis, in which reduced metabolic supply (e.g., reduced glucose and/or oxygen levels), in combination with increased metabolic demand (e.g., due to seizures or periodic discharges) leads to cellular injury (e.g., evidenced by elevation in the lactate/pyruvate ratio, Refs. 46 and 47). Nevertheless, the MSDMH is specified at a conceptual level and does not provide explicit or detailed mechanisms for how the various factors interact. In proposing an explicit mathematical model of the underlying physiological mechanisms, our model attempts to fill this

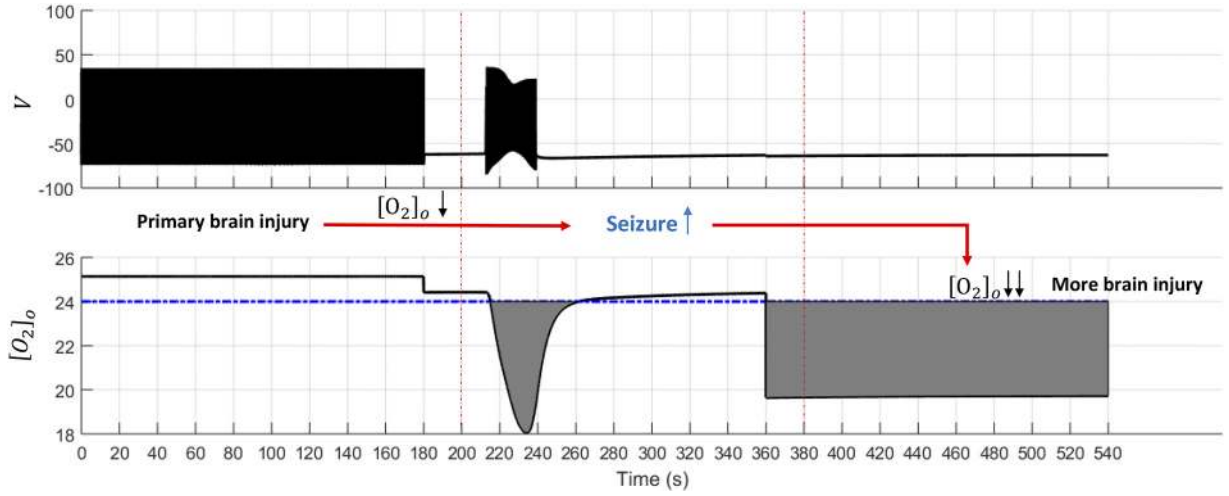

Figure 13. Decreased oxygen levels: third pathway for evolution of primary brain injury (PBI) into secondary brain injury (SBI). Model behavior (reversal potential of K^+, and O_2 concentration) in relation to decreased $[O_2]_{bath}$ induced by the PBI. These observations are summarized in Fig. 10*C*. $[O_2]_o$, extracellular oxygen concentration; *V*, membrane potential.

gap. Our model, based on the Hodgkin–Huxley model, is supplemented with additional dynamics of three known mechanisms in SBI, namely, decreased oxygen, increased extracellular potassium, and increased excitotoxicity. In addition, we define four new indices: hypoxia index (HI), epileptiform activity intensity (EI), quantities of reversal potentials of Na^+ and K^+ ($V_{E_{Na}}$, V_{E_K}). Then, according to the proposed model and the defined indices, we show how changes in extracellular potassium, oxygen concentration, and excitotoxicity might play important roles in the evolution from PBI to SBI and suggest three underlying paths for how events following PBI may lead to SBI.

In contrast to current practices which assume that ischemia plays the predominant role in SBI and that interventions should focus on enhancing delivery of cerebral blood flow and oxygen, our model and the data they are based on (Refs. 48 and 49) suggest that metabolic crisis can also be nonischemic. Thus, our model predicts that commonly used physiologic endpoints [intracranial pressure (ICP) and blood pressure targets], and methods for monitoring these, are insufficient to prevent SBI. A corollary of this prediction is that additional interventions aimed at preventing and controlling seizures and epileptiform activity, reducing inflammation, and preventing excitotoxicity may be needed to optimize prevention of SBI. In turn, biomarkers more directly related to metabolic supply and demand are likely needed to judge the adequacy of medical interventions in patients with SBI. These might include microdialysis (30, 50), tissue oxygen and blood flow (51), and continuous electroencephalography (52).

Various single neuron computational models have been built based on the HH model, augmented with mathematically characterized mechanisms, to elucidate the generation of physio-pathological activities or phenomena. It is worth mentioning here the works of Barreto and Cressman (39), Zandt et al. (53), and Wei et al. (17), where the dynamics of ions (especially potassium and sodium) are characterized the same way as in our work. Although the base model, and the dynamic equation of potassium used in these works are similar to those in our model, the problems addressed in four works are quite different. Barreto and Cressman described a neuron model to show the role of ion concentration dynamics in the generation of periodic bursting behavior. Zandt et al. applied a bifurcation analysis for a single-cell model to explain five different kinds of membrane voltage patterns related to anoxic depolarization in slices of rat cortex. Wei et al. proposed a biophysical model to account for experimental observations that related to seizures and oxygen dynamics. In contrast, our work focuses on explaining how patients with acute brain injury can develop SBI. Due to the different objectives, the final models in four works are also quite different. The work of Barreto and Cressman considered ion concentration dynamics and added additional equations to describe the dynamics of both intra- and extracellular sodium and potassium to the base HH model. The work of Zandt et al. directly replicated the model used in Barreto and Cressman without modification. In the work of Wei et al., the model is an extension of the HH formalism and includes the neuronal microenvironment dynamics of sodium, potassium, and oxygen concentrations. By contrast, the model proposed in our work, based on the base HH model, is supplemented with additional dynamics corresponding to three mechanisms involved in SBI: *1*) decreased oxygen; *2*) increased extracellular potassium; and *3*) increased excitotoxicity. Although we use the same equations for potassium and oxygen as in Barreto and Cressman and Wei et al. in our work, a novel component is that we included dynamics of excitotoxicity in our study. Other novel components are that our model includes a self-reinforcing feedback loop by making the relevant parameter (i.e., $[K^+]_{bath}$, $[O_2]_{bath}$, g_{mean}) a function of EI. Finally, we explicitly identify three underlying paths for how events following PBI may lead to SBI. In addition, our analysis of this model also helps to provide new hypotheses to explain several important empirical observations from prior literature, including the observation that brain injury frequently leads to seizures, and that more severe brain injury is associated with more severe seizures.

Limitations

Our study has important limitations. Most importantly, our results are based on mathematical modeling rather than direct physical experiments. Thus, our work suggests mechanisms to explain relationships and correlations from prior observational studies but does not provide definitive evidence for the proposed mechanisms. Another limitation is that our model does not include all mechanisms that have been proposed to contribute to metabolic supply demand mismatch. In particular, our model does not include inflammation, which may be an important mediator of SBI in subarachnoid hemorrhage (51), nor have we studied the role of cortical spreading depolarizations, which likely also play a critical role in SBI (54). These topics remain for future modeling studies.

In addition, it is necessary to clarify that the frequency of seizures and PDs in our model is not exactly equivalent to some observations reported in the literature. For example, in the work of Witsch et al. (5), it was shown that PDs greater than 2 Hz represent the threshold for hypoxia. Our model agrees with this work qualitatively, but not quantitatively. This is not surprising, given that the frequency of PDs in work of Witsch et al. was computed from scalp EEG which reflects the activity of an assembly of neurons, whereas our model is a simplified computational model. In our work, the frequency of seizures and PDs is computed from a simplified compartment of a single biological neuron. Nevertheless, our work successfully captured the main hypothesis in the work of Witsch et al., which is that the higher-frequency discharges appear to cause increased metabolic stress and more hypoxia than lower frequency discharges.

In addition, it is important to study how the SBI in one region affects SBI in other regions. In future work, we will consider more neurons with excitatory and inhibitory synaptic connections and extend our single neuron model to a network-based model.

Conclusion

We have proposed an explicit neurophysiologically plausible mechanistic model for the metabolic supply demand mismatch hypothesis of SBI. Our model is based on three modifications of the well-studied Hodgkin–Huxley model that are believed central to brain dysfunction in primary

brain injury as it evolves into secondary brain injury: increased extracellular potassium, decreased oxygen concentration, and increased excitotoxity. We defined four new indices to characterize effects of hypoxia, seizure activity, and reversal potentials of Na^+ and K^+ to quantify the extent of secondary injury, epileptiform activity intensity, and the quantity of reversal potentials. Furthermore, according to the proposed model and the defined indices, we explored the relationship among pathological alterations following PBI, seizures, and SBI and provided a high-level unified explanation for why patients with acute brain injury frequently develop SBI. Using this model, we investigated how decreased oxygen, increased extracellular potassium, excitotoxicity, and seizures may induce SBI and suggest three underlying pathways for how events following PBI may lead to SBI. The proposed model helps explain several important empirical observations, including the common association of acute brain injury with seizures, the association of seizures with tissue hypoxia and so on. In contrast to current practices which assume that ischemia plays the predominant role in SBI, our model suggests that metabolic crisis involved in SBI can also be nonischemic.

GRANTS

Drs. J.-L. Song and R. Zhang were supported by the National Natural Science Foundation of China under Grant 62006189, the Innovative Talents Promotion Plan of Shaanxi Province under Grant 2018TD-016, and the Key Research and Development Program of Shaanxi Province under Grant 2019ZDLSF02-09-02. Dr. M. B. Westover is supported by the Glenn Foundation for Medical Research and the American Federation for Aging Research through a Breakthroughs in Gerontology Grant; through the American Academy of Sleep Medicine through an AASM Foundation Strategic Research Award; and by grants from the NIH (1R01NS102190, 1R01NS102574, 1R01NS107291, and 1RF1AG064312). Dr. A. F. Struck was supported by R01-NS1111022-01A1. Dr. J. A. Kim was supported by AAN Clinical Research Training Scholarship and NeuroNEXT Fellowship.

DISCLOSURES

No conflicts of interest, financial or otherwise, are declared by the authors.

AUTHOR CONTRIBUTIONS

J.-L.S., J.A.K., and M.B.W. conceived and designed research; J.-L.S. performed experiments; J.-L.S. analyzed data; J.-L.S., J.A.K., A.F.S., and M.B.W. interpreted results of experiments; J.-L.S. prepared figures; J.-L.S. drafted manuscript; J.-L.S., J.A.K., A.F.S., R.Z., and M.W. edited and revised manuscript; R.Z. and M.B.W. approved final version of manuscript.

REFERENCES

1. **Siesjö BK**, **Katsura K**, **Zhao Q**, **Folbergrová J**, **Pahlmark K**, **Siesjö P**, **Smith ML.** Mechanisms of secondary brain damage in global and focal ischemia: a speculative synthesis. *J Neurotrauma* 12: 943–956, 1995. doi:10.1089/neu.1995.12.943.
2. **Vespa P**, **Bergsneider M**, **Hattori N**, **Wu H-M**, **Huang S-C**, **Martin NA**, **Glenn TC**, **McArthur DL**, **Hovda DA.** Metabolic crisis without brain ischemia is common after traumatic brain injury: a combined microdialysis and positron emission tomography study. *J Cereb Blood Flow Metab* 25: 763–774, 2005. doi:10.1038/sj.jcbfm.9600073.
3. **Vespa PM**, **Miller C**, **McArthur D**, **Eliseo M**, **Etchepare M**, **Hirt D**, **Glenn TC**, **Martin N**, **Hovda D.** Nonconvulsive electrographic seizures after traumatic brain injury result in a delayed, prolonged increase in intracranial pressure and metabolic crisis. *Crit Care Med* 35: 2830–2836, 2007.
4. **Kim JA**, **Rosenthal ES**, **Biswal S**, **Zafar S**, **Shenoy AV**, **O'Connor KL**, **Bechek SC**, **Valdery Moura J**, **Shafi MM**, **Patel AB**, **Cash SS**, **Westover MB.** Epileptiform abnormalities predict delayed cerebral ischemia in subarachnoid hemorrhage. *Clin Neurophysiol* 128: 1091–1099, 2017. doi:10.1016/j.clinph.2017.01.016.
5. **Witsch J**, **Frey H-P**, **Schmidt JM**, **Velazquez A**, **Falo CM**, **Reznik M**, **Roh D**, **Agarwal S**, **Park S**, **Connolly ES**, **Claassen J.** Electroencephalographic periodic discharges and frequency-dependent brain tissue hypoxia in acute brain injury. *JAMA Neurol* 74: 301–309, 2017. doi:10.1001/jamaneurol.2016.5325.
6. **David O**, **Cosmelli D**, **Friston KJ.** Evaluation of different measures of functional connectivity using a neural mass model. *Neuroimage* 21: 659–673, 2004. doi:10.1016/j.neuroimage.2003.10.006.
7. **Schellenberger Costa M**, **Weigenand A**, **Ngo H-VV**, **Marshall L**, **Born J**, **Martinetz T**, **Claussen JC.** A thalamocortical neural mass model of the EEG during NREM sleep and its response to auditory stimulation. *PLoS Comput Biol* 12: e1005022, 2016. doi:10.1371/journal.pcbi.1005022.
8. **Basu I**, **Crocker B**, **Farnes K**, **Robertson MM**, **Paulk AC**, **Vallejo DI**, **Dougherty DD**, **Cash SS**, **Eskandar EN**, **Kramer MM**, **Widge AS.** A neural mass model to predict electrical stimulation evoked responses in human and non-human primate brain. *J Neural Eng* 15: 066012, 2018. doi:10.1088/1741-2552/aae136.
9. **Taher H**, **Torcini A**, **Olmi S.** Exact neural mass model for synaptic-based working memory. *PLoS Comput Biol* 16: e1008533, 2020. doi:10.1371/journal.pcbi.1008533.
10. **Ching S**, **Purdon PL**, **Vijayan S**, **Kopell NJ**, **Brown EN.** A neurophysiological–metabolic model for burst suppression. *Proc Natl Acad Sci USA* 109: 3095–3100, 2012. doi:10.1073/pnas.1121461109.
11. **Cressman JR**, **Ullah G**, **Ziburkus J**, **Schiff SJ**, **Barreto E.** The influence of sodium and potassium dynamics on excitability, seizures, and the stability of persistent states. I. Single neuron dynamics. *J Comput Neurosci* 26: 159–170, 2009 [Erratum in *J Comput Neurosci* 30: 781, 2011]. doi:10.1007/s10827-008-0132-4.
12. **Ingram J**, **Zhang C**, **Cressman JR**, **Hazra A**, **Wei Y**, **Koo YE**, **Žiburkus J**, **Kopelman R**, **Xu J**, **Schiff SJ.** Oxygen and seizure dynamics. I. Experiments. *J Neurophysiol* 112: 205–212, 2014. doi:10.1152/jn.00540.2013.
13. **Raimondo JV**, **Burman RJ**, **Katz AA**, **Akerman CJ.** Ion dynamics during seizures. *Front Cell Neurosci* 9: 419, 2015. doi:10.3389/fncel.2015.00419.
14. **Wei Y**, **Ullah G**, **Schiff SJ.** Unification of neuronal spikes, seizures, and spreading depression. *J Neurosci* 34: 11733–11743, 2014. doi:10.1523/JNEUROSCI.0516-14.2014.
15. **Zhu F**, **Wang R**, **Aihara K**, **Pan X.** Energy-efficient firing patterns with sparse bursts in the Chay neuron model. *Nonlinear Dyn* 100: 2657–2672, 2020. doi:10.1007/s11071-020-05593-8.
16. **Hodgkin AL**, **Huxley AF.** The components of membrane conductance in the giant axon of Loligo. *J Physiol* 116: 473–496, 1952. doi:10.1113/jphysiol.1952.sp004718.
17. **Wei Y**, **Ullah G**, **Ingram J**, **Schiff SJ.** Oxygen and seizure dynamics. II. Computational modeling. *J Neurophysiol* 112: 213–223, 2014. doi:10.1152/jn.00541.2013.
18. **Kubota M**, **Nakamura T**, **Sunami K**, **Ozawa Y**, **Namba H**, **Yamaura A**, **Makino H.** Changes of local cerebral glucose utilization, DC potential and extracellular potassium concentration in experimental head injury of varying severity. *Neurosurg Rev* 12, *Suppl* 1: 393–399, 1989. doi:10.1007/BF01790681.
19. **Cozzolino O**, **Marchese M**, **Trovato F**, **Pracucci E**, **Ratto GM**, **Buzzi MG**, **Sicca F**, **Santorelli FM.** Understanding spreading depression from headache to sudden unexpected death. *Front Neurol* 9: 19, 2018. doi:10.3389/fneur.2018.00019.
20. **Hamming AM**, **Wermer MJH**, **Umesh Rudrapatna S**, **Lanier C**, **van Os HJA**, **van den Bergh WM**, **Ferrari MD**, **van der Toorn A**, **van den Maagdenberg A**, **Stowe AM**, **Dijkhuizen RM.** Spreading depolarizations increase delayed brain injury in a rat model of subarachnoid

hemorrhage. *J Cereb Blood Flow Metab* 36: 1224–1231, 2016. doi:10.1177/0271678X15619189.

21. **Hayes RL**, **Katayama Y**, **Young HF**, **Dunbar JG.** Coma associated with flaccidity produced by fluid-percussion concussion in the cat. I. Is it due to depression of activity within the brainstem reticular formation? *Brain Inj* 2: 31–49, 1988. doi:10.3109/02699058809150930.
22. **Bergsneider M**, **Hovda DA**, **McArthur DL**, **Etchepare M**, **Huang SC**, **Sehati N**, **Satz P**, **Phelps ME**, **Becker DP.** Metabolic recovery following human traumatic brain injury based on FDG-PET: time course and relationship to neurological disability. *J Head Trauma Rehabil* 16: 135–148, 2001. doi:10.1097/00001199-200104000-00004.
23. **Martin WRW**, **Baker RP**, **Grubb RL**, **Raichle ME.** Cerebral blood volume, blood flow, and oxygen metabolism in cerebral ischaemia and subarachnoid haemorrhage: an in-vivo study using positron emission tomography. *Acta Neurochir (Wien)* 70: 3–9, 1984. doi:10.1007/BF01406037.
24. **Xia S**, **Utriainen D**, **Tang J**, **Kou Z**, **Zheng G**, **Wang X**, **Shen W**, **Haacke EM**, **Lu G.** Decreased oxygen saturation in asymmetrically prominent cortical veins in patients with cerebral ischemic stroke. *Magn Reson Imaging* 32: 1272–1276, 2014. doi:10.1016/j.mri.2014.08.012.
25. **Hayes RL**, **Jenkins LW**, **Lyeth BG.** Neurotransmitter mediated mechanisms of traumatic brain injury: acetylcholine and excitatory amino acids. *J Neurotrauma* 9, *Suppl* 1: 173–187, 1992.
26. **Katayama Y**, **Becker DP**, **Tamura T**, **Hovda DA.** Massive increases in extracellular potassium and the indiscriminate release of glutamate following concussive brain injury. *J Neurosurg* 73: 889–900, 1990. doi:10.3171/jns.1990.73.6.0889.
27. **Faden AI**, **Demediuk P**, **Panter SS**, **Vink R.** The role of excitatory amino acids and NMDA receptors in traumatic brain injury. *Science* 244: 798–800, 1989. doi:10.1126/science.2567056.
28. **Bretón RR**, **Rodríguez JCG** (Editors)**.** Excitotoxicity and oxidative stress in acute ischemic stroke. In: *Acute Ischemic Stroke*. Croatia: University Campus, 2012, vol. 200, p. 29–58. doi:10.5772/64991.
29. **Wang C**, **Ji B**, **Cheng B**, **Chen J**, **Bai BO.** Neuroprotection of microRNA in neurological disorders. *Biomed Rep* 2: 611–619, 2014. doi:10.3892/br.2014.297.
30. **Vespa P**, **Tubi M**, **Claassen J**, **Buitrago-Blanco M**, **McArthur D**, **Velazquez AG**, **Tu B**, **Prins M**, **Nuwer M.** Metabolic crisis occurs with seizures and periodic discharges after brain trauma. *Ann Neurol* 79: 579–590, 2016. doi:10.1002/ana.24606.
31. **De Marchis GM**, **Pugin D**, **Meyers E**, **Velasquez A**, **Suwatcharangkoon S**, **Park S**, **Falo MC**, **Agarwal S**, **Mayer S**, **Schmidt JM**, **Connolly ES**, **Claassen J.** Seizure burden in subarachnoid hemorrhage associated with functional and cognitive outcome. *Neurology* 86: 253–260, 2016. doi:10.1212/WNL.0000000000002281.
32. **Lucke-Wold BP**, **Nguyen L**, **Turner RC**, **Logsdon AF**, **Chen Y-W**, **Smith KE**, **Huber JD**, **Matsumoto R**, **Rosen CL**, **Tucker ES**, **Richter E.** Traumatic brain injury and epilepsy: underlying mechanisms leading to seizure. *Seizure* 33: 13–23, 2015. doi:10.1016/j.seizure.2015.10.002.
33. **Rodriguez Ruiz AR**, **Vlachy J**, **Lee JW**, **Gilmore EJ**, **Ayer T**, **Haider HA**, **Gaspard N**, **Ehrenberg JA**, **Tolchin B**, **Fantaneanu TA**, **Fernandez A**, **Hirsch LJ**, **LaRoche S**; **Critical Care EEG Monitoring Research Consortium.** Association of periodic and rhythmic electroencephalographic patterns with seizures in critically ill patients. *JAMA Neurol* 74: 181–188, 2017. doi:10.1001/jamaneurol.2016.4990.
34. **Struck AF**, **Ustun B**, **Ruiz AR**, **Lee JW**, **LaRoche SM**, **Hirsch LJ**, **Gilmore EJ**, **Vlachy J**, **Haider HA**, **Rudin C**, **Westover MB.** Association of an electroencephalography-based risk score with seizure probability in hospitalized patients. *JAMA Neurol* 74: 1419–1424, 2017. doi:10.1001/jamaneurol.2017.2459.
35. **Claassen J.** How I treat patients with EEG patterns on the ictal–interictal continuum in the neuro ICU. *Neurocrit Care* 11: 437–444, 2009. doi:10.1007/s12028-009-9295-8.
36. **Bazhenov M**, **Timofeev I**, **Steriade M**, **Sejnowski TJ.** Potassium model for slow (2–3 Hz) in vivo neocortical paroxysmal oscillations. *J Neurophysiol* 92: 1116–1132, 2004. doi:10.1152/jn.00529.2003.
37. **Penny WD**, **Friston KJ**, **Ashburner JT**, **Kiebel SJ**, **Nichols TE** (Editors)**.** *Statistical Parametric Mapping: The Analysis of Functional Brain Images*. London: Academic Press, 2011.
38. **Destexhe A**, **Rudolph M**, **Fellous JM**, **Sejnowski TJ.** Fluctuating synaptic conductances recreate in vivo-like activity in neocortical neurons. *Neuroscience* 107: 13–24, 2001. doi:10.1016/S0306-4522(01)00344-X.
39. **Barreto E**, **Cressman JR.** Ion concentration dynamics as a mechanism for neuronal bursting. *J Biol Phys* 37: 361–373, 2011. doi:10.1007/s10867-010-9212-6.
40. **Paulson OB**, **Newman EA**, **Paulson OB**, **Newman EA.** Does the release of potassium from astrocyte endfeet regulate cerebral blood flow? *Science* 237: 896–898, 1987. doi:10.1126/science.3616619.
41. **Gloor SM.** Relevance of Na,K-ATPase to local extracellular potassium homeostasis and modulation of synaptic transmission. *FEBS Lett* 412: 1–4, 1997. doi:10.1016/S0014-5793(97)00774-6.
42. **Galeffi F**, **Somjen GG**, **Foster KA**, **Turner DA.** Simultaneous monitoring of tissue PO_2 and NADH fluorescence during synaptic stimulation and spreading depression reveals a transient dissociation between oxygen utilization and mitochondrial redox state in rat hippocampal slices. *J Cereb Blood Flow Metab* 31: 626–639, 2011. doi:10.1038/jcbfm.2010.136.
43. **Dingledine R**, **Borges K**, **Bowie D**, **Traynelis SF.** The glutamate receptor ion channels. *Pharmacol Rev* 51: 7–61, 1999.
44. **Hofmeijer J**, **Tjepkema-Cloostermans MC**, **van Putten MJ.** Burst-suppression with identical bursts: a distinct EEG pattern with poor outcome in postanoxic coma. *Clin Neurophysiol* 125: 947–954, 2014. doi:10.1016/j.clinph.2013.10.017.
45. **Crino PB**, **Jin H**, **Shumate MD**, **Robinson MB**, **Coulter DA**, **Brooks-Kayal AR.** Increased expression of the neuronal glutamate transporter (EAAT3/EAAC1) in hippocampal and neocortical epilepsy. *Epilepsia* 43: 211–218, 2002. doi:10.1046/j.1528-1157.2002.35001.x.
46. **Wu H-M**, **Huang S-C**, **Hattori N**, **Glenn TC**, **Vespa PM**, **Hovda DA**, **Bergsneider M.** Subcortical white matter metabolic changes remote from focal hemorrhagic lesions suggest diffuse injury after human traumatic brain injury. *Neurosurgery* 55: 1306–1315, 2004. doi:10.1227/01.NEU.0000143028.08719.42.
47. **Bilotta F**, **Caramia R**, **Cernak I**, **Paoloni FP**, **Doronzio A**, **Cuzzone V**, **Santoro A**, **Rosa G.** Intensive insulin therapy after severe traumatic brain injury: a randomized clinical trial. *Neurocrit Care* 9: 159–166, 2008. doi:10.1007/s12028-008-9084-9.
48. **Bergsneider M**, **Hovda DA**, **Shalmon E**, **Kelly DF**, **Vespa PM**, **Martin NA**, **Phelps ME**, **McArthur DL**, **Caron MJ**, **Kraus JF**, **Becker DP.** Cerebral hyperglycolysis following severe traumatic brain injury in humans: a positron emission tomography study. *J Neurosurg* 86: 241–251, 1997. doi:10.3171/jns.1997.86.2.0241.
49. **Huang SC**, **Phelps ME**, **Hoffman EJ**, **Sideris K**, **Selin CJ**, **Kuhl DE.** Noninvasive determination of local cerebral metabolic rate of glucose in man. *Am J Physiol Endocrinol Metab* 238: E69–E82, 1980. doi:10.1152/ajpendo.1980.238.1.E69.
50. **Vespa P**, **McArthur DL**, **Stein N**, **Huang S-C**, **Shao W**, **Filippou M**, **Etchepare M**, **Glenn T**, **Hovda DA.** Tight glycemic control increases metabolic distress in traumatic brain injury: a randomized controlled within-subjects trial. *Crit Care Med* 40: 1923–1929, 2012. doi:10.1097/CCM.0b013e31824e0fcc.
51. **Claassen J**, **Perotte A**, **Albers D**, **Kleinberg S**, **Schmidt JM**, **Tu B**, **Badjatia N**, **Lantigua H**, **Hirsch LJ**, **Mayer SA**, **Connolly ES**, **Hripcsak G.** Nonconvulsive seizures after subarachnoid hemorrhage: multimodal detection and outcomes. *Ann Neurol* 74: 53–64, 2013. doi:10.1002/ana.23859.
52. **Struck AF**, **Osman G**, **Rampal N**, **Biswal S**, **Legros B**, **Hirsch LJ**, **Westover MB**, **Gaspard N.** Time-dependent risk of seizures in critically ill patients on continuous electroencephalogram. *Ann Neurol* 82: 177–185, 2017. doi:10.1002/ana.24985.
53. **Zandt B-J**, **Stigen T**, **Ten Haken B**, **Netoff T**, **van Putten MJAM.** Single neuron dynamics during experimentally induced anoxic depolarization. *J Neurophysiol* 110: 1469–1475, 2013. doi:10.1152/jn.00250.2013.
54. **Hartings JA**, **Strong AJ**, **Fabricius M**, **Manning A**, **Bhatia R**, **Dreier JP**, **Mazzeo AT**, **Tortella FC**, **Bullock MR**; **Co-Operative Study of Brain Injury Depolarizations.** Spreading depolarizations and late secondary insults after traumatic brain injury. *J Neurotrauma* 26: 1857–1866, 2009. doi:10.1089/neu.2009.0961.